

# Reduced Absorption Due to Defect-Localized Interlayer Excitons in Transition-Metal Dichalcogenide–Graphene Heterostructures

Daniel Hernangómez-Pérez,\* Amir Kleiner, and Sivan Refaelly-Abramson\*



Cite This: *Nano Lett.* 2023, 23, 5995–6001



Read Online

ACCESS |

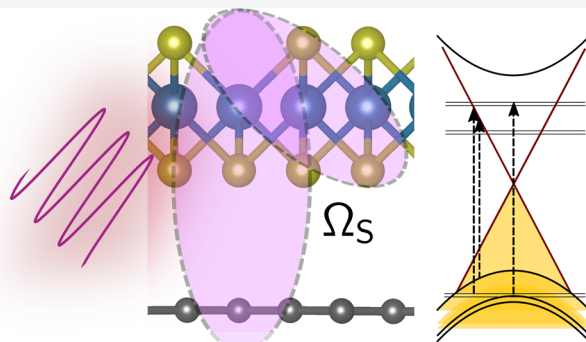
Metrics & More

Article Recommendations

Supporting Information

**ABSTRACT:** Associating atomic vacancies to excited-state transport phenomena in two-dimensional semiconductors demands a detailed understanding of the exciton transitions involved. We study the effect of such defects on the electronic and optical properties of WS<sub>2</sub>–graphene and MoS<sub>2</sub>–graphene van der Waals heterobilayers, employing many-body perturbation theory. We find that chalcogen defects and the graphene interface radically alter the optical properties of the transition-metal dichalcogenide in the heterobilayer, due to a combination of dielectric screening and the many-body nature of defect-induced intralayer and interlayer optical transitions. By analyzing the intrinsic radiative rates of the subgap excitonic features, we show that while defects introduce low-lying optical transitions, resulting in excitons with non-negligible oscillator strength, they decrease the optical response of the pristine-like transition-metal dichalcogenide intralayer excitons. Our findings relate excitonic features with interface design for defect engineering in photovoltaic and transport applications.

**KEYWORDS:** 2D materials, transition-metal dichalcogenides, heterostructures, defects, graphene, excitons



Van der Waals heterostructures,<sup>1–4</sup> formed by vertically stacking atomically thin two-dimensional layers through weak interlayer interactions, are considered some of the most promising systems for the next generation of ultrathin optoelectronic and photovoltaic high-performance components with tunable properties and tailored functionalities modifiable at the atomic scale.<sup>5–10</sup> An important example of such heterostructures is the heterobilayer formed by stacking graphene<sup>11,12</sup> with a monolayer transition-metal dichalcogenide (TMDC) of the type XSe<sub>2</sub>, where X is W or Mo.<sup>13–18</sup> These are type I heterostructures which combine the high carrier mobility,<sup>19</sup> high thermal conductivity,<sup>20</sup> and semi-metallic character of graphene with pseudospin circular dichroism,<sup>21–23</sup> large quantum confinement, strong light absorption properties,<sup>24</sup> and sizable spin-orbit interaction of a direct band gap TMDC.<sup>25,26</sup>

The electronic and optical properties of layered TMDCs and their heterostructures are sensitive to the potential created by defects.<sup>27–31</sup> In particular, the most abundant and stable point defects in these systems are monatomic chalcogen vacancies.<sup>32–34</sup> Electron–hole optical transitions between the defect and pristine states are known to produce novel subgap excitonic features<sup>28,35–39</sup> and form localized excitons that were shown to intrinsically reduce the degree of valley polarization even without additional scattering mechanisms.<sup>28,36,40–42</sup> Furthermore, changes in the dielectric environment can impact the TMDC intrinsic light emission properties.<sup>43–45</sup> For instance, interlayer coupling between graphene and TMDC

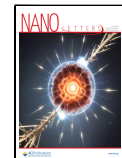
results in a notable quenching of excitonic photoluminescence<sup>46</sup> or an increase of the exciton line width.<sup>47</sup> Engineering the exciton spontaneous decay time is also possible by microcavity formation by additional adsorbed layers and the consequent Purcell effect.<sup>48,49</sup> This effect has been shown to give low-temperature picosecond exciton photoresponses. Therefore, and due to the defect's ubiquitous nature, a microscopic understanding of the emergent electronic and excitonic properties of TMDC–graphene (Gr) heterobilayers in the presence of vacancies is interesting for dynamic modeling of optoelectronic devices and applications.

In this work, we investigate the electronic and optical properties of WS<sub>2</sub>–Gr and MoS<sub>2</sub>–Gr heterobilayers with monatomic chalcogen vacancies. We employ a GW-BSE approach<sup>50–56</sup> to compute the many-body electronic properties and optical characteristics and find that due to the combination of screening and strong optical hybridization, absorption resonances of well-known pristine TMDC excitons are strongly quenched in the heterostructure, resulting in substantially altered absorbance properties compared to the

Received: March 29, 2023

Revised: June 15, 2023

Published: June 22, 2023



pristine TMDC–Gr heterobilayer or defected TMDC without graphene. These pristine-like TMDC “A” and “B” peaks are largely reduced due to the mixing of the optical transitions with both graphene and defect electronic states, and the electron–hole transitions determining their excitonic composition are fundamentally altered. This manifests also in a strong reduction of the excitonic binding energy for the excitons composing those absorption peaks. In addition, Fermi-level alignment of the defect transition levels and the magnitude of the spin–orbit interaction, determined by the choice of TMDC, lead to substantial changes in the heterostructure optical properties. We obtain the intrinsic radiative rates for excitons with the largest binding energy, which create strongly mixed subgap resonances and show that the associated inverse rates are comparable to those calculated for pristine TMDC monolayers.

We employ a commensurate supercell composed of  $4 \times 4$  WS<sub>2</sub> (respectively MoS<sub>2</sub>) and  $5 \times 5$  graphene elementary cells; see Figure 1a and the Supporting Information (SI). We consider a vacancy concentration of  $\sim 3\%$ , corresponding to an isolated monoatomic sulfur vacancy per supercell, located at

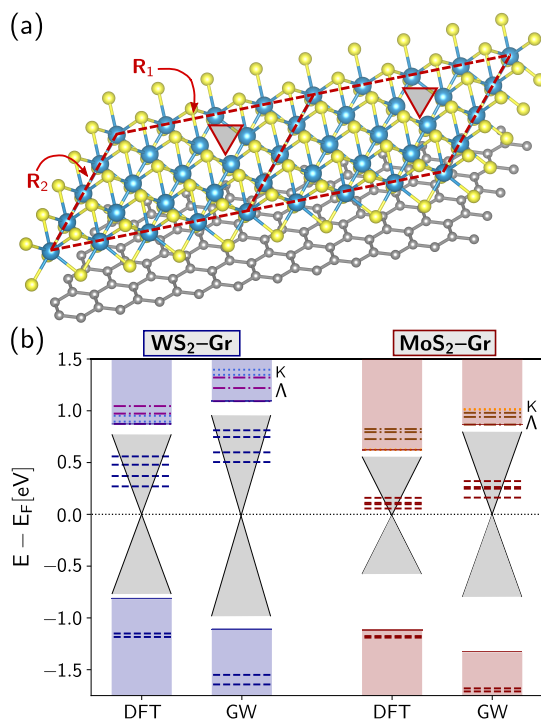


**Figure 1.** (a) Schematics of the defected WS<sub>2</sub>–Gr heterobilayer. Each supercell (two are shown here) forms a parallelepiped with lateral boundaries marked by the straight red lines (in-plane supercell lattice vectors are denoted by  $\mathbf{R}_1$  and  $\mathbf{R}_2$ ). The monoatomic chalcogen vacancy position, located opposite to the graphene layer, is indicated by a red triangle. (b) DFT and GW calculated valence and conduction band energies at the  $\bar{K}$  point. The blue bars on the left-hand side correspond to WS<sub>2</sub>–Gr and the red bars on the right-hand side to MoS<sub>2</sub>–Gr. The dashed lines denote the defect energy levels, and the solid lines mark the top of the pristine TMDC valence and conduction bands. Energies are related to the Dirac point of graphene,  $E_F$ , which sets the Fermi energy of the system. The gray sketch of the Dirac cone represents the region of the TMDC pristine band gap occupied by graphene. Conduction levels with predominantly  $\Lambda$  nature are represented by the dashed-dotted lines, with those with predominantly  $K$  nature represented by dotted lines.

the opposite side of the graphene layer with sufficiently small interactions between defect sites at neighboring periodic replicas of the supercell.<sup>17</sup> We first perform a geometry optimization of the supercell atomic positions, keeping the supercell volume constant (see ref 17 and the SI). This optimization reduces the nearest-neighbor bonds close to the vacancy (which shrinks and strains the TMDC lattice) as well as the interlayer distance between the TMDC and the graphene layer. Using DFT as a starting point (with the PBE functional<sup>57</sup>), we perform a one-shot GW ( $G_0W_0$ ) calculation for each TMDC–Gr heterobilayer (see computational details in the SI). Figure 1b shows the DFT and GW energies at the point  $\bar{K}$  of the supercell Brillouin zone in an energy level diagram. As expected based on previous studies,<sup>28,58,59</sup> GW quasi-particle corrections increase the gap in both systems, qualitatively, conserving the DFT picture for these heterobilayers.<sup>17</sup> There are four spin–orbit split defect states shifted upon the GW calculation to higher energy with respect to the Fermi level. Far from the Fermi level, we find the valence band splitting due to spin–orbit interaction to be  $\sim 460$  meV for WS<sub>2</sub>–Gr and 150 meV for MoS<sub>2</sub>–Gr, which is consistent with  $425 \pm 18$  and  $170 \pm 2$  meV obtained from high-resolution ARPES measurements.<sup>26</sup> The dielectric screening also shifts the pair of occupied defect states to lower energies (by  $\sim 400$ –450 meV for WS<sub>2</sub>–Gr and  $\sim 400$  meV for MoS<sub>2</sub>–Gr). Simultaneously, the pristine-like band gap of WS<sub>2</sub> increases from 1.69 eV at the DFT level to 2.20 eV at the GW level. Similarly, the pristine-like band gap of MoS<sub>2</sub>–Gr changes from 1.73 to 2.19 eV. These values reflect a significant renormalization of the TMDC band gaps compared to the monolayer case, as expected due to the quasi-metallic character of graphene with GW corrections including image charge effects.<sup>59</sup> Our GW results are in agreement with previous calculations with a reported band gap reduction of  $\sim 300$ –350 meV<sup>59,60</sup> compared to each pristine counterpart.<sup>58</sup> They are also consistent with the experimental values of the quasi-particle band gap found in MoS<sub>2</sub>–Gr heterostructures, reported to be  $\sim 2.0$ –2.2 eV,<sup>61,62</sup> and in WS<sub>2</sub>–Gr, which is in the range  $\sim 2.0$ –2.3 eV.<sup>14,63,64</sup>

Next, we examine the excitonic properties of defected WS<sub>2</sub>–Gr and MoS<sub>2</sub>–Gr heterobilayers using the Bethe–Salpeter equation<sup>54,55</sup> within the Tamm–Dancoff approximation (see the SI). We show in Figure 2, top panel, the absorbance of WS<sub>2</sub>–Gr as well as its decomposition into intralayer graphene, intralayer TMDC, and interlayer contributions (see the SI for the case of MoS<sub>2</sub>–Gr). At low optical energies, intralayer graphene electron–hole excitonic features are found to be the most prominent. Graphene electronic intraband transitions (not considered in our calculations, as well as temperature effects) are known to dominate this regime,<sup>65</sup> which is marked by a dashed gray rectangle. The resonant peaks are a consequence of the finite  $k$ -grid sampling of the graphene Dirac cone, and therefore, the absorption in this region is actually continuous in the dense grid limit. In the high infrared spectral range, excitonic peaks corresponding to interlayer graphene–defect and graphene–pristine optical transitions appear at higher energies while graphene intralayer contributions become less relevant. At optical energies  $\gtrsim 2.0$  eV, intralayer TMDC contributions (in the form of defect–defect, defect–pristine, and pristine–pristine band transitions) become the dominant features of the spectrum over the interlayer contributions. Out of all optical transitions sampled for the examined  $k$ -grid and energy range, 0.4% belong to

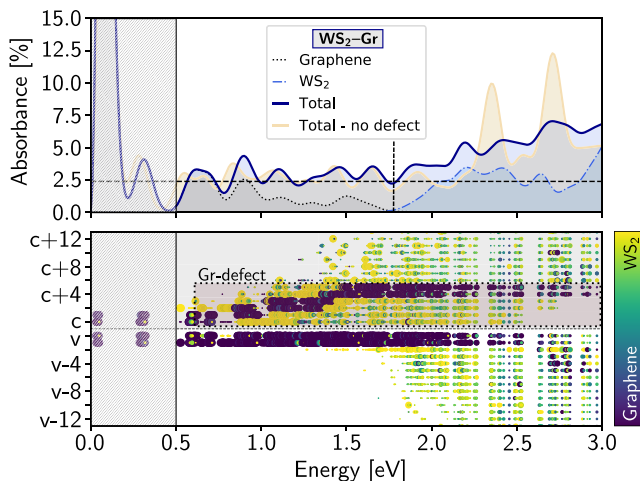


**Figure 2.** Absorbance and exciton contributions for the defected  $\text{WS}_2\text{-Gr}$  heterobilayer. (top) Absorbance calculated along one of the main in-plane polarization directions as well as its decomposition into intralayer graphene and  $\text{WS}_2$  contributions (interlayer contributions are read from the difference between the three traces). For comparison, we also show the absorbance of the pristine  $\text{WS}_2\text{-Gr}$  heterobilayer. The dashed horizontal black line marks the 2.4% universal limit of graphene absorbance at the infrared energies. The shaded box represents the estimated range for which we expect a smooth and monotonic spectrum dominated by graphene (instead of resonances resulting from finite  $\mathbf{k}$ -grid sampling). The vertical dotted line marks the optical ranges below which excitons are dominated by defect-graphene subgap transitions to a range where excitons present larger intralayer TMDC composition. (bottom) For each exciton composing the absorbance resonances, we represent the contribution of each electron and hole band. Each dot corresponds to the band contribution to a given exciton summed over all  $\mathbf{k}$  points (only bright contributions whose oscillator strength are  $>5$  a.u. are shown). For clarity, all dots with values  $\geq 10^3$  a.u. have the same area. The color code corresponds to the layer composition of each contribution, and the dotted box marks the graphene-defect empty bands.

intralayer graphene, while 62% correspond to intralayer TMDC transitions, with the remaining 37% representing a large degree of interlayer mixing.

The spectral absorbance of graphene for infrared light is almost constant at 2.4%.<sup>65–71</sup> This limit is represented by a dashed horizontal line in Figure 2. We find that absorbance resonances in the optical range between  $\sim 1.0$  and  $1.6$  eV oscillate around values larger than the graphene infrared constant limit. This is associated with excitons that involve defects and should persist in the dense grid limit. The computed absorbance values in this range are also consistent with those calculated for defected  $\text{MoSe}_2$  in the absence of graphene.<sup>28</sup> To further validate our findings, we compare the absorbance spectra of  $\text{WS}_2\text{-Gr}$  with and without vacancies. We observe that, unlike the defected heterostructure, the absorbance of the pristine heterobilayer oscillates around the graphene limit in that energy range, supporting our previous conclusion. In the visible range (i.e.,  $\sim 1.6\text{--}3.2$  eV), experiments on  $\text{WS}_2$  have reported a red shift and a significant reduction of the exciton peak area upon graphene stacking.<sup>47,72</sup> These effects are typically attributed to both changes in the dielectric environment upon the heterostructure formation and possible interfacial charge transfer.<sup>73</sup> Our results demonstrate that within the exciton basis set, optical transitions at both layers mix already upon light absorption. In defected  $\text{WS}_2\text{-Gr}$  heterobilayers, we observe a reduction of the strength of the

pristine-like TMDC resonances in addition to the substantial interlayer mixing in the subgap optical region dominated by transitions to the defect states. This effect is attributed to the strong optical mixing of TMDC and graphene, which results in additional interlayer optical transitions. These occur within the pristine gap at many different  $\mathbf{k}$ -points due to the dispersive nature of the Dirac cone and yield a redistribution of the oscillator strength from the original pristine transitions to the defects. These combined effects of the graphene and vacancies quench the pristine-like “A” and “B” resonances<sup>74,75</sup> and also broaden them.<sup>41</sup> As a consequence, they are no longer as dominant in the spectrum. Moreover, the composition of the absorption peaks, clearly defined at  $\sim 2.2$ ,  $\sim 2.4$ , and  $\sim 2.7$  eV, also changes drastically compared to the expectation for the pristine or defected TMDC monolayers (see the SI).

To further understand this effect, we show in Figure 2, bottom panel, the contribution of each band to the exciton (similarly to our previous analysis of exciton state mixing in defected systems<sup>28,36,76</sup>). Each excitonic state,  $|\Psi^S\rangle$ , defined by its wave function amplitude  $A_{vck}^S$  and energy  $\Omega_S$ , is represented by a column of dots whose area is proportional to  $\sum_{vck} |A_{vck}^S|^2$ , for each electron band ( $c$ ), and  $\sum_{vck} |A_{vck}^S|^2$ , for each hole band ( $v$ ). The color of the dot represents the layer from which  $c$  or from which  $v$  the transitions occur. We observe intralayer graphene optical transitions in the low energy region ( $\lesssim 0.5$  eV), while excitonic resonances with interlayer character appear only above 0.5 eV. The dispersive nature of graphene can be seen from the increase in the conduction band number of graphene with energy. As expected, the quenched high-energy resonances show significant contribution of mixed TMDC and graphene optical transitions; thus, although they appear in similar positions, they no longer possess true “A” and “B” characters (see the SI). We note that while the increase of the dielectric screening by the surrounding media and the reduction of the absorbance is expected,<sup>64</sup> here the effect is further pronounced due to the electron–hole defect and nondefect mixing in the subgap region.

The binding energy of the exciton quantifies how strongly bound the electrons and holes participating in the excitation are. Intralayer graphene excitonic features have vanishing small binding energies ( $\sim 0\text{--}1$  meV, see also refs 65 and 77) despite their strong oscillator strength. This differs significantly from pristine or encapsulated TMDC excitons, which have a large oscillator strength and binding energies. In particular, experimental estimations of the binding energies are 0.3–0.4 eV for  $\text{MoS}_2$  and 0.3–0.7 eV for  $\text{WS}_2$  pristine “A” excitons.<sup>78</sup> Theoretical predictions give 0.6 eV for  $\text{MoS}_2$  and 0.2 eV for  $\text{WS}_2$  pristine “B” excitons.<sup>75</sup> In Figure 3a, we present the exciton energy as a function of the binding energy for  $\text{WS}_2\text{-Gr}$  (see the SI for  $\text{MoS}_2\text{-Gr}$ ). The binding energy is computed from the energy difference between the free and bound electron-hole pairs composing each exciton (see SI). For excitons in the optical region where the pristine “A” and “B” resonances would be expected, we observe that excitons have substantially lower binding energies compared to the pristine or encapsulated counterparts, as well as substantially smaller oscillator strengths. We attribute this to a redistribution of the oscillator strength due to the combined effect of substantial hybridization of the defect and nondefect electron–hole transitions with graphene, as well as the small binding properties of excitons in graphene resulting from its quasi-metallic nature at low energies. Importantly, we also find excitons (with oscillator strength in the range  $10^{-2}\text{--}1.0$  a.u.) in

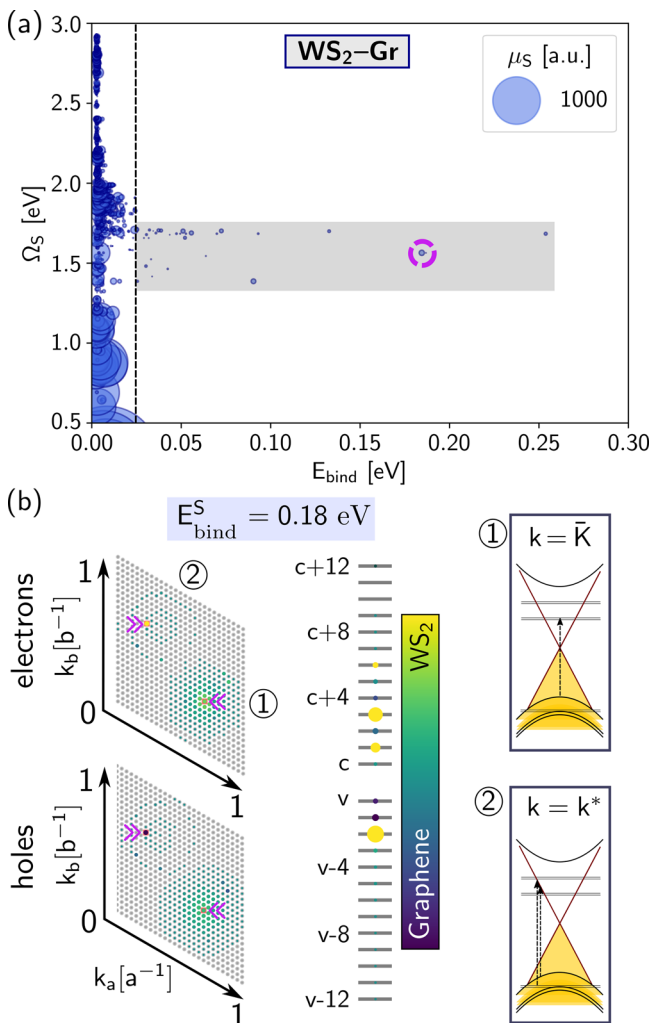


**Figure 3.** (a) Exciton energies for  $\text{WS}_2\text{-Gr}$ ,  $\Omega_s$  as a function of their binding energy,  $E_{\text{bind}}$ . Only excitons for which  $E_{\text{bind}} > 2.5$  meV are shown (~8000 out of 142884 excitons for our  $k$ -grid sampling and bands). The size of each dot is proportional to the oscillator strength,  $\mu_s$ . Bright excitons, in particular those dominated by intralayer graphene transitions, have very small binding energies (smaller than the thermal energy at room temperature, marked by a dashed black vertical line). Excitons within the energy range where the pristine “A” and “B” features would be expected are dark and have a very small binding energy. The gray rectangle corresponds to excitons with binding energies larger than 25 meV. (b) Brillouin zone exciton distribution and transition band diagram for the exciton marked with a purple circle in (a). The top Brillouin zone corresponds to transitions to the conduction bands, and the bottom one corresponds to transitions from the valence bands. On the right-hand side schematics, we show selected transitions marked by ① and ② at the  $k$ -points indicated by purple arrows.

the optical region 1.5–2.0 eV with a binding energy comparable to that of pristine excitons in the absence of a graphene layer. These excitons result from intralayer optical transitions to defect states and interlayer graphene–defect transitions. To gain insight into the nature of these excitons, we show in Figure 3b the  $k$ -space distribution for a representative case marked by a circle in Figure 3a. It is worth noting that their degree of localization cannot be used to infer the strength of the binding, as excitons with similar binding may exhibit optical transitions in very different regions of the Brillouin zone due to the dispersive nature of the

graphene bands and the delocalization of defect states in  $k$ -space. The right-hand side of Figure 3b displays the optical transitions at selected  $k$ -points, supporting our analysis that this exciton is formed by a combination of defect–defect (notably at  $\bar{K}$ ), graphene–valence, and graphene–defect transitions (for the  $k$ -point noted as  $k^*$ ).

Finally, we relate our findings to the intrinsic radiative decay rates of zero-momentum excitons, which can be computed from the GW-BSE oscillator strength and excitation energy.<sup>79–81</sup> We consider the inverse rate, which scales as  $\gamma_s^{-1} := \tau_s \approx \Omega_s/\mu_s$ . This rate accounts only for part of the radiative line width, as other contributions, e.g. electron–phonon and exciton–phonon terms, are not included, and is useful to evaluate the significance of the oscillator strength. Our analysis reveals that the inverse rates for the excitons with binding  $>50$  meV can be as large as  $\tau_s \approx 0.1$  ps for both heterobilayers. However, depending on the oscillator strength, they can be shorter, even as small as  $\tau_s \approx 0.1$  fs for  $\text{MoS}_2\text{-Gr}$  (see the SI). Intralayer graphene excitonic features, which have significantly small binding, have substantially larger intrinsic rates due to their large optical transition dipole. Dark interlayer excitons with large binding have larger inverse rates, as large as ~100 ps for  $\text{WS}_2\text{-Gr}$ , due to the smaller oscillator strength. For pristine  $\text{WS}_2\text{-Gr}$  bright “A” and “B” excitons in the TMDC layer,  $\tau_s$  can be even shorter, essentially due to the increased oscillator strength (between 2 and 3 orders of magnitude compared to the defect-related excitons, see the SI) which yields  $\tau_s \approx 10^{-4}\text{--}10^{-5}$  fs. We note that compared to pristine TMDCs,<sup>80</sup> graphene adsorption has a strong impact on  $\tau_s$ , which only become comparable again to the pristine ones in the presence of defects due to the strong exciton hybridization of the graphene and the subgap vacancy-related features. Furthermore, charge transfer times of photocarriers at TMDC–graphene interfaces,<sup>13–15,82,83</sup> where single-particle defect tunneling is understood to be the dominating coherent transport channel,<sup>14,17</sup> can be of a similar order of magnitude. In this scenario, defects slow down coherent charge transfer due to relatively small interlayer tunneling. Interestingly, in the presence of graphene, defects optically enhance transitions associated with them, resulting in excitons with significantly higher oscillator strength, compared to the reduced oscillator strength of the original pristine-like “A” and “B” TMDC excitons.

In conclusion, we have studied the electronic and optical properties of  $\text{WS}_2\text{-Gr}$  and  $\text{MoS}_2\text{-Gr}$  heterobilayers with chalcogen vacancies by employing first-principles many-body perturbation theory. We find that strong hybridization of the defect states with graphene gives rise to subgap features, which manifest as strong resonances in the optical absorbance spectrum, while quenching the “A” and “B” pristine exciton peaks originally coming from intralayer TMDC transitions. These altered absorption features may be used to extend the functionality in the infrared of solar cells. We have analyzed the stability of the excitons and found a strong reduction of the binding energy for those TMDC excitons, while strongly hybridized interlayer and defect-dominated excitons have binding energies up to ~250 meV. We computed the intrinsic radiative decay rate of these excitons and found inverse rates of up to 0.1 ps. Overall, our results demonstrate how point-like defects can be used to design optical features in graphene-based van der Waals heterostructures, where excitons inherit properties from two well-distinct layers in a nontrivial way, pointing to the relevance of a first-principles understanding of

many-body effects in the description of these systems for transport and potential optoelectronic applications.

## ■ ASSOCIATED CONTENT

### § Supporting Information

The Supporting Information is available free of charge at <https://pubs.acs.org/doi/10.1021/acs.nanolett.3c01182>.

Computational details and methods, additional results, convergence checks, absorbance, and additional results for MoS<sub>2</sub>–Gr, wave function density of relevant conduction states, exciton reciprocal space composition for relevant energies in the WS<sub>2</sub>–Gr spectra, and additional figures ([PDF](#))

## ■ AUTHOR INFORMATION

### Corresponding Authors

Daniel Hernangómez-Pérez – Department of Molecular Chemistry and Materials Science, Weizmann Institute of Science, Rehovot 7610001, Israel;  [orcid.org/0000-0002-4277-0236](http://orcid.org/0000-0002-4277-0236); Email: [daniel.hernangomez@weizmann.ac.il](mailto:daniel.hernangomez@weizmann.ac.il)

Sivan Refaely-Abramson – Department of Molecular Chemistry and Materials Science, Weizmann Institute of Science, Rehovot 7610001, Israel;  [orcid.org/0000-0002-7031-8327](http://orcid.org/0000-0002-7031-8327); Email: [sivan.refaely-abramson@weizmann.ac.il](mailto:sivan.refaely-abramson@weizmann.ac.il)

### Author

Amir Kleiner – Department of Molecular Chemistry and Materials Science, Weizmann Institute of Science, Rehovot 7610001, Israel;  [orcid.org/0000-0003-0738-2729](http://orcid.org/0000-0003-0738-2729)

Complete contact information is available at:

<https://pubs.acs.org/10.1021/acs.nanolett.3c01182>

### Notes

The authors declare no competing financial interest.

## ■ ACKNOWLEDGMENTS

The authors acknowledge Tomer Amit, María Camarasa-Gómez, Diana Qiu, Alexey Chernikov, Florian Dirnberger, Paulo E. Faria Junior, and Alexander Holleitner for insightful discussions. The authors are thankful to Simone Latini, Lede Xian, and Angel Rubio for the initial geometry employed as a starting point of the calculations performed in this manuscript. The computations were carried out in the Chemfarm local cluster at the Weizmann Institute of Science and the Max Planck Computing and Data Facility cluster. D.H.-P. and A.K. acknowledge the Minerva Foundation grant 7135421. This research was supported by the German Research Foundation (DFG) through the Collaborative Research Center SFB 1277 (Project-ID 314695032, project B10). S.R.-A. is an incumbent of the Leah Omenn Career Development Chair. This project has received funding from the European Research Council (ERC), Grant agreement No. 101041159.

## ■ REFERENCES

- (1) Wang, Q. H.; Kalantar-Zadeh, K.; Kis, A.; Coleman, J. N.; Strano, M. S. Electronics and optoelectronics of two-dimensional transition metal dichalcogenides. *Nature Nanotechnology* **2012**, *7*, 699–712.
- (2) Geim, A. K.; Grigorieva, I. V. Van der Waals heterostructures. *Nature* **2013**, *499*, 419–425.
- (3) Novoselov, K. S.; Mishchenko, A.; Carvalho, A.; Castro Neto, A. H. 2D materials and van der Waals heterostructures. *Science* **2016**, *353*, aac9439.
- (4) Liu, Y.; Weiss, N. O.; Duan, X.; Cheng, H.-C.; Huang, Y.; Duan, X. Van der Waals heterostructures and devices. *Nature Reviews Materials* **2016**, *1*, 16042.
- (5) Radisavljevic, B.; Radenovic, A.; Brivio, J.; Giacometti, V.; Kis, A. Single-layer MoS<sub>2</sub> transistors. *Nature Nanotechnology* **2011**, *6*, 147–150.
- (6) Lopez-Sanchez, O.; Lembke, D.; Kayci, M.; Radenovic, A.; Kis, A. Ultrasensitive photodetectors based on monolayer MoS<sub>2</sub>. *Nature Nanotechnology* **2013**, *8*, 497–501.
- (7) Ross, J. S.; Klement, P.; Jones, A. M.; Ghimire, N. J.; Yan, J.; Mandrus, D. G.; Taniguchi, T.; Watanabe, K.; Kitamura, K.; Yao, W.; Cobden, D. H.; Xu, X. Electrically tunable excitonic light-emitting diodes based on monolayer WSe<sub>2</sub> p-n junctions. *Nature Nanotechnology* **2014**, *9*, 268–272.
- (8) Jariwala, D.; Sangwan, V. K.; Lauhon, L. J.; Marks, T. J.; Hersam, M. C. Emerging device applications for semiconducting two-dimensional transition metal dichalcogenides. *ACS Nano* **2014**, *8*, 1102–1120.
- (9) Pospischil, A.; Furchi, M. M.; Mueller, T. Solar-energy conversion and light emission in an atomic monolayer p-n diode. *Nature Nanotechnology* **2014**, *9*, 257–261.
- (10) De Fazio, D.; Goykhman, I.; Yoon, D.; Bruna, M.; Eiden, A.; Milana, S.; Sassi, U.; Barbone, M.; Dumcenco, D.; Marinov, K.; Kis, A.; Ferrari, A. C. High responsivity, large-area graphene/MoS<sub>2</sub> flexible photodetectors. *ACS Nano* **2016**, *10*, 8252–8262.
- (11) Novoselov, K. S.; Geim, A. K.; Morozov, S. V.; Jiang, D.; Katsnelson, M. I.; Grigorieva, I. V.; Dubonos, S. V.; Firsov, A. A. Two-dimensional gas of massless Dirac fermions in graphene. *Nature* **2005**, *438*, 197–200.
- (12) Castro Neto, A. H.; Guinea, F.; Peres, N. M. R.; Novoselov, K. S.; Geim, A. K. The electronic properties of graphene. *Rev. Mod. Phys.* **2009**, *81*, 109–162.
- (13) Aeschlimann, S.; Rossi, A.; Chávez-Cervantes, M.; Krause, R.; Arnoldi, B.; Stadtmüller, B.; Aeschlimann, M.; Forti, S.; Fabbri, F.; Coletti, C.; Gierz, I. Direct evidence for efficient ultrafast charge separation in epitaxial WS<sub>2</sub>/graphene heterostructures. *Science Advances* **2020**, *6*, 1.
- (14) Krause, R.; Aeschlimann, S.; Chávez-Cervantes, M.; Pereira-Causin, R.; Brem, S.; Malic, E.; Forti, S.; Fabbri, F.; Coletti, C.; Gierz, I. Microscopic understanding of ultrafast charge transfer in van der Waals heterostructures. *Phys. Rev. Lett.* **2021**, *127*, 276401.
- (15) Fu, S.; du Fosse, I.; Jia, X.; Xu, J.; Yu, X.; Zhang, H.; Zheng, W.; Krasel, S.; Chen, Z.; Wang, Z. M.; Tielrooij, K.-J.; Bonn, M.; Houtepen, A. J.; Wang, H. I. Long-lived charge separation following pump-wavelength-dependent ultrafast charge transfer in graphene/WS<sub>2</sub> heterostructures. *Science Advances* **2021**, *7*, eabd9061.
- (16) Devidas, T. R.; Keren, I.; Steinberg, H. Spectroscopy of NbSe<sub>2</sub> using energy-tunable defect-embedded quantum dots. *Nano Letters* **2021**, *21*, 6931–6937.
- (17) Hernangómez-Pérez, D.; Donarini, A.; Refaely-Abramson, S. Charge quenching at defect states in transition metal dichalcogenide-graphene van der Waals heterobilayers. *Phys. Rev. B* **2023**, *107*, 075419.
- (18) Faria, P. E., Jr.; Naimer, T.; McCreary, K. M.; Jonker, B. T.; Finley, J. J.; Crooker, S. A.; Fabian, J.; Stier, A. V. Proximity-enhanced valley Zeeman splitting at the WS<sub>2</sub>/graphene interface. *2D Materials* **2023**, *10*, 034002.
- (19) Mayorov, A. S.; Gorbachev, R. V.; Morozov, S. V.; Britnell, L.; Jalil, R.; Ponomarenko, L. A.; Blake, P.; Novoselov, K. S.; Watanabe, K.; Taniguchi, T.; Geim, A. K. Micrometer-scale ballistic transport in encapsulated graphene at room temperature. *Nano Letters* **2011**, *11*, 2396–2399.
- (20) Balandin, A. A.; Ghosh, S.; Bao, W.; Calizo, I.; Teweldebrhan, D.; Miao, F.; Lau, C. N. Superior thermal conductivity of single-layer graphene. *Nano Letters* **2008**, *8*, 902–907.

- (21) Yao, W.; Xiao, D.; Niu, Q. Valley-dependent optoelectronics from inversion symmetry breaking. *Phys. Rev. B* **2008**, *77*, 235406.
- (22) Cao, T.; Wang, G.; Han, W.; Ye, H.; Zhu, C.; Shi, J.; Niu, Q.; Tan, P.; Wang, E.; Liu, B.; Feng, J. Valley-selective circular dichroism of monolayer molybdenum disulphide. *Nature Communications* **2012**, *3*, 887.
- (23) Ye, Z.; Sun, D.; Heinz, T. F. Optical manipulation of valley pseudospin. *Nature Physics* **2017**, *13*, 26–29.
- (24) Bernardi, M.; Palummo, M.; Grossman, J. C. Extraordinary sunlight absorption and one nanometer thick photovoltaics using two-dimensional monolayer materials. *Nano Letters* **2013**, *13*, 3664–3670.
- (25) Zhu, Z. Y.; Cheng, Y. C.; Schwingenschlögl, U. Giant spin-orbit-induced spin splitting in two-dimensional transition-metal dichalcogenide semiconductors. *Phys. Rev. B* **2011**, *84*, 153402.
- (26) Latzke, D. W.; Zhang, W.; Suslu, A.; Chang, T.-R.; Lin, H.; Jeng, H.-T.; Tongay, S.; Wu, J.; Bansil, A.; Lanzara, A. Electronic structure, spin-orbit coupling, and interlayer interaction in bulk MoS<sub>2</sub> and WS<sub>2</sub>. *Phys. Rev. B* **2015**, *91*, 235202.
- (27) Aghajanian, M.; Mostofi, A. A.; Lischner, J. Tuning electronic properties of transition-metal dichalcogenides via defect charge. *Sci. Rep.* **2018**, *8*, 13611.
- (28) Refaelly-Abramson, S.; Qiu, D. Y.; Louie, S. G.; Neaton, J. B. Defect-induced modification of low-lying excitons and valley selectivity in monolayer transition metal dichalcogenides. *Phys. Rev. Lett.* **2018**, *121*, 167402.
- (29) Schuler, B.; Qiu, D. Y.; Refaelly-Abramson, S.; Kastl, C.; Chen, C. T.; Barja, S.; Koch, R. J.; Ogletree, D. F.; Aloni, S.; Schwartzberg, A. M.; Neaton, J. B.; Louie, S. G.; Weber-Bargioni, A. Large spin-orbit splitting of deep in-gap defect states of engineered sulfur vacancies in monolayer WS<sub>2</sub>. *Phys. Rev. Lett.* **2019**, *123*, 076801.
- (30) Barja, S.; Refaelly-Abramson, S.; Schuler, B.; Qiu, D. Y.; Pulkkinen, A.; Wickenburg, S.; Ryu, H.; Ugeda, M. M.; Kastl, C.; Chen, C.; Hwang, C.; Schwartzberg, A.; Aloni, S.; Mo, S.-K.; Frank Ogletree, D.; Crommie, M. F.; Yazyev, O. V.; Louie, S. G.; Neaton, J. B.; Weber-Bargioni, A. Identifying substitutional oxygen as a prolific point defect in monolayer transition metal dichalcogenides. *Nature communications* **2019**, *10*, 3382.
- (31) Aghajanian, M.; Schuler, B.; Cochrane, K. A.; Lee, J.-H.; Kastl, C.; Neaton, J. B.; Weber-Bargioni, A.; Mostofi, A. A.; Lischner, J. Resonant and bound states of charged defects in two-dimensional semiconductors. *Phys. Rev. B* **2020**, *101*, 081201.
- (32) Zhou, W.; Zou, X.; Najmaei, S.; Liu, Z.; Shi, Y.; Kong, J.; Lou, J.; Ajayan, P. M.; Yakobson, B. I.; Idrobo, J.-C. Intrinsic structural defects in monolayer molybdenum disulfide. *Nano Letters* **2013**, *13*, 2615–2622.
- (33) Liu, D.; Guo, Y.; Fang, L.; Robertson, J. Sulfur vacancies in monolayer MoS<sub>2</sub> and its electrical contacts. *Appl. Phys. Lett.* **2013**, *103*, 183113.
- (34) Noh, J.-Y.; Kim, H.; Kim, Y.-S. Stability and electronic structures of native defects in single-layer MoS<sub>2</sub>. *Phys. Rev. B* **2014**, *89*, 205417.
- (35) Attaccalite, C.; Bockstedte, M.; Marini, A.; Rubio, A.; Wirtz, L. Coupling of excitons and defect states in boron-nitride nanostructures. *Phys. Rev. B* **2011**, *83*, 144115.
- (36) Mitterreiter, E.; Schuler, B.; Micevic, A.; Hernangomez-Perez, D.; Barthelmi, K.; Cochrane, K. A.; Kiemle, J.; Sigger, F.; Klein, J.; Wong, E.; Barnard, E. S.; Watanabe, K.; Taniguchi, T.; Lorke, M.; Jahnke, F.; Finley, J. J.; Schwartzberg, A. M.; Qiu, D. Y.; Refaelly-Abramson, S.; Holleitner, A. W.; Weber-Bargioni, A.; Kastl, C. The role of chalcogen vacancies for atomic defect emission in MoS<sub>2</sub>. *Nature Communications* **2021**, *12*, 3822.
- (37) Hotger, A.; Klein, J.; Barthelmi, K.; Sigl, L.; Sigger, F.; Manner, W.; Gyger, S.; Florian, M.; Lorke, M.; Jahnke, F.; Taniguchi, T.; Watanabe, K.; Jons, K. D.; Wurstbauer, U.; Kastl, C.; Muller, K.; Finley, J. J.; Holleitner, A. W. Gate-switchable arrays of quantum light emitters in contacted monolayer MoS<sub>2</sub> van der Waals heterostructures. *Nano Letters* **2021**, *21*, 1040–1046.
- (38) Sigger, F.; Amersdorffer, I.; Hotger, A.; Nutz, M.; Kiemle, J.; Taniguchi, T.; Watanabe, K.; Forg, M.; Noe, J.; Finley, J. J.; Hogege, A.; Holleitner, A. W.; Hummer, T.; Hunger, D.; Kastl, C. Ultra-sensitive extinction measurements of optically active defects in monolayer MoS<sub>2</sub>. *The Journal of Physical Chemistry Letters* **2022**, *13*, 10291–10296.
- (39) Micevic, A.; Pettinger, N.; Hötger, A.; Sigl, L.; Florian, M.; Taniguchi, T.; Watanabe, K.; Müller, K.; Finley, J. J.; Kastl, C.; Holleitner, A. W. On-demand generation of optically active defects in monolayer WS<sub>2</sub> by a focused helium ion beam. *Appl. Phys. Lett.* **2022**, *121*, 183101.
- (40) Chow, P. K.; Jacobs-Gedrim, R. B.; Gao, J.; Lu, T.-M.; Yu, B.; Terrones, H.; Koratkar, N. Defect-induced photoluminescence in monolayer Ssemitconducting transition metal dichalcogenides. *ACS Nano* **2015**, *9*, 1520–1527.
- (41) Amit, T.; Hernangomez-Perez, D.; Cohen, G.; Qiu, D. Y.; Refaelly-Abramson, S. Tunable magneto-optical properties in MoS<sub>2</sub> via defect-induced exciton transitions. *Phys. Rev. B* **2022**, *106*, L161407.
- (42) Hötger, A.; Amit, T.; Klein, J.; Barthelmi, K.; Pelini, T.; Delhomme, A.; Rey, S.; Potemski, M.; Faugeras, C.; Cohen, G.; Hernangómez-Pérez, D.; Taniguchi, T.; Watanabe, K.; Kastl, C.; Finley, J. J.; Refaelly-Abramson, S.; Holleitner, A. W.; Stier, A. V. Spin-defect characteristics of single sulfur vacancies in monolayer MoS<sub>2</sub>. *npj 2D Materials and Applications* **2023**, *7*, 30.
- (43) Steinhoff, A.; Kim, J.-H.; Jahnke, F.; Rösner, M.; Kim, D.-S.; Lee, C.; Han, G. H.; Jeong, M. S.; Wehling, T. O.; Gies, C. Efficient exciton photoluminescence in direct and indirect band gap monolayer MoS<sub>2</sub>. *Nano Letters* **2015**, *15*, 6841–6847.
- (44) Wang, H.; Zhang, C.; Chan, W.; Manolatou, C.; Tiwari, S.; Rana, F. Radiative lifetimes of excitons and trions in monolayers of the metal dichalcogenide MoS<sub>2</sub>. *Phys. Rev. B* **2016**, *93*, 045407.
- (45) Robert, C.; Lagarde, D.; Cadiz, F.; Wang, G.; Lassagne, B.; Amand, T.; Balocchi, A.; Renucci, P.; Tongay, S.; Urbaszek, B.; Marie, X. Exciton radiative lifetime in transition metal dichalcogenide monolayers. *Phys. Rev. B* **2016**, *93*, 205423.
- (46) Lorchat, E.; Lopez, L. E. P.; Robert, C.; Lagarde, D.; Froehlicher, G.; Taniguchi, T.; Watanabe, K.; Marie, X.; Berciaud, S. Filtering the photoluminescence spectra of atomically thin semiconductors with graphene. *Nature Nanotechnology* **2020**, *15*, 283–288.
- (47) Hill, H. M.; Rigosi, A. F.; Raja, A.; Chernikov, A.; Roquelet, C.; Heinz, T. F. Exciton broadening in WS<sub>2</sub>/graphene heterostructures. *Phys. Rev. B* **2017**, *96*, 205401.
- (48) Massicotte, M.; Schmidt, P.; Vialla, F.; Schädler, K. G.; Reserbat-Plantey, A.; Watanabe, K.; Taniguchi, T.; Tielrooij, K. J.; Koppens, F. H. L. Picosecond photoresponse in van der Waals heterostructures. *Nature Nanotechnology* **2016**, *11*, 42–46.
- (49) Fang, H. H.; Han, B.; Robert, C.; Semina, M. A.; Lagarde, D.; Courtade, E.; Taniguchi, T.; Watanabe, K.; Amand, T.; Urbaszek, B.; Glazov, M. M.; Marie, X. Control of the exciton radiative lifetime in van der Waals heterostructures. *Phys. Rev. Lett.* **2019**, *123*, 067401.
- (50) Hedin, L. New method for calculating the one-particle Green's function with application to the electron-gas problem. *Phys. Rev.* **1965**, *139*, A796–A823.
- (51) Hybertsen, M. S.; Louie, S. G. First-principles theory of quasiparticles: Calculation of band gaps in semiconductors and insulators. *Phys. Rev. Lett.* **1985**, *55*, 1418–1421.
- (52) Hybertsen, M. S.; Louie, S. G. Electron correlation in semiconductors and insulators: Band gaps and quasiparticle energies. *Phys. Rev. B* **1986**, *34*, 5390–5413.
- (53) Albrecht, S.; Reining, L.; Onida, G.; Del Sole, R. Computing optical absorption spectra from first principles: Self-energy and electron-hole interaction effects. *Il Nuovo Cimento D* **1998**, *20*, 949–956.
- (54) Rohlfing, M.; Louie, S. G. Electron-hole excitations in semiconductors and insulators. *Phys. Rev. Lett.* **1998**, *81*, 2312–2315.
- (55) Rohlfing, M.; Louie, S. G. Electron-hole excitations and optical spectra from first principles. *Phys. Rev. B* **2000**, *62*, 4927–4944.
- (56) Deslippe, J.; Samsonidze, G.; Strubbe, D. A.; Jain, M.; Cohen, M. L.; Louie, S. G. BerkeleyGW: A massively parallel computer package for the calculation of the quasiparticle and optical properties

- of materials and nanostructures. *Comput. Phys. Commun.* **2012**, *183*, 1269–1289.
- (57) Perdew, J. P.; Burke, K.; Ernzerhof, M. Generalized gradient approximation made simple. *Phys. Rev. Lett.* **1996**, *77*, 3865–3868.
- (58) Qiu, D. Y.; da Jornada, F. H.; Louie, S. G. Optical spectrum of MoS<sub>2</sub>: Many-body effects and diversity of exciton states. *Phys. Rev. Lett.* **2013**, *111*, 216805.
- (59) Naik, M. H.; Jain, M. Substrate screening effects on the quasiparticle band gap and defect charge transition levels in MoS<sub>2</sub>. *Phys. Rev. Materials* **2018**, *2*, 084002.
- (60) Jin, C.; Rasmussen, F. A.; Thygesen, K. S. Tuning the Schottky barrier at the graphene/MoS<sub>2</sub> interface by electron doping: density functional theory and many-body calculations. *The Journal of Physical Chemistry C* **2015**, *119*, 19928–19933.
- (61) Shi, J.; Liu, M.; Wen, J.; Ren, X.; Zhou, X.; Ji, Q.; Ma, D.; Zhang, Y.; Jin, C.; Chen, H.; Deng, S.; Xu, N.; Liu, Z.; Zhang, Y. All chemical vapor deposition synthesis and intrinsic bandgap observation of MoS<sub>2</sub>/graphene heterostructures. *Adv. Mater.* **2015**, *27*, 7086–7092.
- (62) Liu, X.; Balla, I.; Bergeron, H.; Campbell, G. P.; Bedzyk, M. J.; Hersam, M. C. Rotationally commensurate growth of MoS<sub>2</sub> on epitaxial graphene. *ACS Nano* **2016**, *10*, 1067–1075.
- (63) Giusca, C. E.; Lin, Z.; Terrones, M.; Gaskell, D. K.; Myers-Ward, R. L.; Kazakova, O. Probing exciton species in atomically thin WS<sub>2</sub>–graphene heterostructures. *Journal of Physics: Materials* **2019**, *2*, 025001.
- (64) Raja, A.; Chaves, A.; Yu, J.; Arefe, G.; Hill, H. M.; Rigosi, A. F.; Berkelbach, T. C.; Nagler, P.; Schuller, C.; Korn, T.; Nuckolls, C.; Hone, J.; Brus, L. E.; Heinz, T. F.; Reichman, D. R.; Chernikov, A. Coulomb engineering of the bandgap and excitons in two-dimensional materials. *Nature Communications* **2017**, *8*, 15251.
- (65) Yang, L.; Deslippe, J.; Park, C.-H.; Cohen, M. L.; Louie, S. G. Excitonic effects on the optical response of graphene and bilayer graphene. *Phys. Rev. Lett.* **2009**, *103*, 186802.
- (66) Nair, R. R.; Blake, P.; Grigorenko, A. N.; Novoselov, K. S.; Booth, T. J.; Stauber, T.; Peres, N. M. R.; Geim, A. K. Fine structure constant defines visual transparency of graphene. *Science* **2008**, *320*, 1308–1308.
- (67) Mak, K. F.; Sfeir, M. Y.; Wu, Y.; Lui, C. H.; Misewich, J. A.; Heinz, T. F. Measurement of the optical conductivity of graphene. *Phys. Rev. Lett.* **2008**, *101*, 196405.
- (68) Gusynin, V. P.; Sharapov, S. G. Transport of Dirac quasiparticles in graphene: Hall and optical conductivities. *Phys. Rev. B* **2006**, *73*, 245411.
- (69) Peres, N. M. R.; Guinea, F.; Castro Neto, A. H. Electronic properties of disordered two-dimensional carbon. *Phys. Rev. B* **2006**, *73*, 125411.
- (70) Nicol, E. J.; Carbotte, J. P. Optical conductivity of bilayer graphene with and without an asymmetry gap. *Phys. Rev. B* **2008**, *77*, 155409.
- (71) Stauber, T.; Peres, N. M. R.; Geim, A. K. Optical conductivity of graphene in the visible region of the spectrum. *Phys. Rev. B* **2008**, *78*, 085432.
- (72) Magnozzi, M.; Ferrera, M.; Piccinini, G.; Pace, S.; Forti, S.; Fabbri, F.; Coletti, C.; Bisio, F.; Canepa, M. Optical dielectric function of two-dimensional WS<sub>2</sub> on epitaxial graphene. *2D Materials* **2020**, *7*, 025024.
- (73) Dong, S., et al. Observation of ultrafast interfacial Meitner-Auger energy transfer in a van der Waals heterostructure, 2022, arXiv:2108.06803, <https://arxiv.org/abs/2108.06803> (accessed May 23, 2023).
- (74) Ramasubramaniam, A. Large excitonic effects in monolayers of molybdenum and tungsten dichalcogenides. *Phys. Rev. B* **2012**, *86*, 115409.
- (75) Druppel, M.; Deilmann, T.; Noky, J.; Marauhn, P.; Kruger, P.; Rohlfing, M. Electronic excitations in transition metal dichalcogenide monolayers from an LDA + GdW approach. *Phys. Rev. B* **2018**, *98*, 155433.
- (76) Steinitz-Eliyahu, R.; Hernangomez-Perez, D.; Hegner, F. S.; Nikacevic, P.; Lopez, N.; Refaeli-Abramson, S. Mixed excitonic nature in water-oxidized BiVO<sub>4</sub> surfaces with defects. *Phys. Rev. Materials* **2022**, *6*, 065402.
- (77) Yang, L. Excitons in intrinsic and bilayer graphene. *Phys. Rev. B* **2011**, *83*, 085405.
- (78) Wang, G.; Chernikov, A.; Glazov, M. M.; Heinz, T. F.; Marie, X.; Amand, T.; Urbaszek, B. Colloquium: Excitons in atomically thin transition metal dichalcogenides. *Rev. Mod. Phys.* **2018**, *90*, 021001.
- (79) Spataru, C. D.; Ismail-Beigi, S.; Capaz, R. B.; Louie, S. G. Theory and ab initio calculation of radiative lifetime of excitons in semiconducting carbon nanotubes. *Phys. Rev. Lett.* **2005**, *95*, 247402.
- (80) Palummo, M.; Bernardi, M.; Grossman, J. C. Exciton radiative lifetimes in two-dimensional transition metal dichalcogenides. *Nano Letters* **2015**, *15*, 2794–2800.
- (81) Chen, H.-Y.; Palummo, M.; Sangalli, D.; Bernardi, M. Theory and ab initio computation of the anisotropic light emission in monolayer transition metal dichalcogenides. *Nano Letters* **2018**, *18*, 3839–3843.
- (82) Jin, C.; Ma, E. Y.; Karni, O.; Regan, E. C.; Wang, F.; Heinz, T. F. Ultrafast dynamics in van der Waals heterostructures. *Nature Nanotechnology* **2018**, *13*, 994–1003.
- (83) Yuan, L.; Chung, T.-F.; Kuc, A.; Wan, Y.; Xu, Y.; Chen, Y. P.; Heine, T.; Huang, L. Photocarrier generation from interlayer charge-transfer transitions in WS<sub>2</sub>-graphene heterostructures. *Science Advances* **2018**, *4*, 1 DOI: [10.1126/sciadv.1700324](https://doi.org/10.1126/sciadv.1700324).

## □ Recommended by ACS

### Quasiparticle and Optical Properties of Carrier-Doped Monolayer MoTe<sub>2</sub> from First Principles

Aurélie Champagne, Jeffrey B. Neaton, et al.

MAY 09, 2023  
NANO LETTERS

READ ▶

### Identification of Exciton Complexes in Charge-Tunable Janus W<sub>Se</sub><sup>s</sup> Monolayers

Matthew S. G. Feuer, Mete Atatüre, et al.  
APRIL 14, 2023  
ACS NANO

READ ▶

### “Dead” Exciton Layer and Exciton Anisotropy of Bulk MoS<sub>2</sub> Extracted from Optical Measurements

Vasyl G. Kravets, Alexander N. Grigorenko, et al.  
NOVEMBER 09, 2022  
ACS NANO

READ ▶

### Ultrafast Thermionic Electron Injection Effects on Exciton Formation Dynamics at a van der Waals Semiconductor/Metal Interface

Kilian R. Keller, Nicolò Maccaferri, et al.  
JULY 20, 2022  
ACS PHOTONICS

READ ▶

Get More Suggestions >